

Multi-Volume High Resolution RGB-D Mapping with Dynamic Volume Placement

Michael Salvato¹, Ross Finman¹, and John J. Leonard¹

I. ABSTRACT

Abstract—We present a novel RGB-D mapping system for generating 3D maps over spatially extended regions with higher resolution than current methods using multiple, dynamically placed mapping volumes. Our method takes in RGB-D frames and dynamically assigns multiple mapping volumes to the environment, exchanging mapping volumes between the CPU and GPU. Mapping volumes are added or removed as needed to allow for spatially extended, high resolution mapping. Our system is designed to maximize the resolution possible for such volumetric methods, while working on an unbounded space.

II. INTRODUCTION

Simultaneous Localization and Mapping (SLAM), is an important task for robotics for applications such as navigation, path planning, and obstacle avoidance. A robot that performs SLAM should be able to create a map of an unknown environment and localize itself within the map as it traverses. The importance of the problem has led to extensive research over the past few decades.

With advances in RGB-D cameras, visual SLAM methods have improved to construct dense RGB-D maps in real time using GPU hardware, leading to advances in not only mapping but more generally in robotic perception. A common method is KinectFusion [1], which popularized dense reconstruction for a predefined volume in real time. Other methods [2], [3] have modified the KinectFusion algorithm to be spatially extended for mapping larger, building-scale environments instead of a predefined volume. Such methods allow for millimeter level reconstructions of the world.

Dense mapping has created a data domain for uses beyond traditional SLAM and allow for applications such as object discovery and detection [4], [5], as well as motion planning [6]. Such applications would still benefit from higher density representations, but the resolution of current methods is limited by the capacity of RAM on the GPU.

In this work, we propose a method allows for one to maximize the resolution of models obtainable by volumetric method such as those in [8]. We provide for the ability to increase resolution of different areas, depending on the requirements of the application. We build on the KinectFusion method by placing multiple small volumes that, due to their

This work was partially supported by the Office of Naval Research under grants N00014-10-1-0936, N00014-11-1-0688 and N00014-13-1-0588 and by the National Science Foundation under grant IIS-1318392, which we gratefully acknowledge.

¹M. Salvato, R. Finman, and J. J. Leonard are with the Computer Science and Artificial Intelligence Laboratory (CSAIL), Massachusetts Institute of Technology (MIT), Cambridge, MA 02139, USA. {msalvato, rfinman, jleonard}@mit.edu



Fig. 1: **Top:** A colored model of the ICL-NUIM Livingroom dataset [7]. **Bottom:** A reconstruction of the same scene with segments showing regions mapped by a volume. Each volume has the maximum resolution that can be loaded into GPU RAM. Volumes are dynamically placed so they are only computed where from the camera is.

reduced physical dimensions, have higher resolution over a smaller patch of the world (See Fig. 1). Each smaller volume is passed in and out of the GPU memory as needed for mapping. Such a method can produce identical results to KinectFusion with unbounded GPU RAM. We then propose a dynamic volume allocation method that both provides higher resolution where it is needed, based on user defined parameters and allows for spatially extended regions. By adding new volumes and removing old ones, the mapping space can be dynamically changed as the camera moves through the world.

In this paper, we present two primary contributions:

- 1) A novel high resolution mapping system using multiple mapping volumes to achieve maximally dense reconstructions.
- 2) A volume placement method for spatially extended

mapping and dynamic resolution modifications based on the environment.

We will also release an open source implementation built off of PCL Kinfu [9].

The paper is structured as follows. First, we discuss related work in the field and how our approach differs. Second, we detail how our multi-volume high resolution mapping method works. Third, we describe our dynamic volume allocation method. Last, we evaluate our work against the state-of-the-art and show how our method has similar accuracy with higher resolution.

III. RELATED WORK

Dense reconstruction methods have become popular since RGB-D sensors have become ubiquitous. While visual SLAM systems were developed before RGB-D sensors [10] and there is much work in monocular SLAM [11]–[13], we will cover only the more recent dense RGB-D SLAM methods here.

There has been significant literature in RGB-D Mapping [14]–[19]. Henry *et. al* [20] introduced one of the first RGB-D mapping algorithms. Their method makes a surfel map of the environment by using visual features and geometric tracking to construct a pose graph. Feature-based methods continue to be a popular approach [21], though many feature-based methods do not take full advantage of the entirety of the data, which can produce improved results in reconstruction [12].

There have been several keyframe-based approaches for RGB-D mapping. Tykkala *et. al* [22] fuses new camera data into an existing keyframe model until a new pose is added. Meilland *et. al* [23] presents an impressive system building on their previous work [24], [25] that combines both the benefits of keyframe and volumetric-based mapping representations. Their method works for large-scale environments in a memory efficient manner. In order to represent the 3D features of a small cluttered scene many small keyframes are required, which could potentially cause tracking drift or failure.

There have been many extensions to KinectFusion, primarily allowing for extending the mapping region beyond a static volume [2], [3]. Whelan *et. al* presents a similar method to our own which extends KinectFusion by moving the TSDF volume through space by utilizing a circular buffer on the GPU. This extends the high resolution capability to building-scale environments. However, this method is still resolution constrained by GPU RAM. Other work on dense RGB-D camera tracking was done by Steinbruecker *et. al* [26], estimating a warping function between an image’s geometric and photometric information and building an octree-based TSDF on a GPU. By using an octree representation building on [27], the system can easily handle multiple resolutions and can be used in conjunction with our work. These methods exploit both the capabilities for the CPU and the GPU to balance the computation load effectively for real time mapping. Chen *et. al* [28] use a hierarchical structure an efficient memory passing between GPU and CPU to minimize

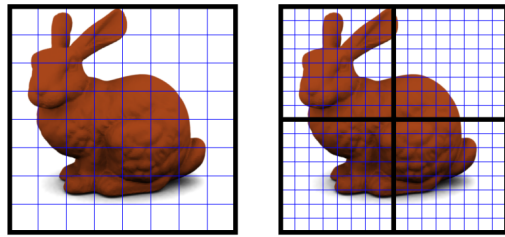


Fig. 2: **Left:** 2D representation of KinectFusion volume with 8 linear voxels scanning a bunny. **Right:** Four volumes each with eight linear voxels scanning a bunny of the same size. In this case we see that we double the linear resolution by using four volumes each with half the length.

unnecessary computation, but requires domain knowledge to determine the correct hierarchical parameters. Nießner *et. al* [29] present a powerful voxel hashing method for large speed up. However they do not support dynamic resolution modification, and through hashing potentially remove data and thus do not guarantee optimal point-wise estimation.

Henry *et. al* [30] uses small patch volumes to segment a mapped space into manageable chunks. Each patch volume is modeled as an independent signed distance function (SDF) and the patches are used for handling loop closures. Having multiple SDFs is similar to our own method, but they use the SDFs for consistent loop closures after they have mapped a scene and not for mapping.

IV. HIGH RESOLUTION MAPPING

We are trying to solve the problem of using a series of depth maps to reconstruct the maximum resolution 3D model that generates those depth maps. As all points read by the camera are noisy, this can be viewed as attempting to find the center of the probability distribution over measurements for each point, while maximizing the number of points modeled. Here we present the problem more precisely based on the input and output relationship, metrics.

A. Input and Output

Our algorithm is designed to output the 3D reconstruction of a fixed size cubic region of physical space using a sequence of provided depth maps. The input to the algorithm is therefore as follows:

- The linear dimension, $l \in \mathbb{R}^+$, of the physical region to be scanned. Our region is assumed to be a cube, so this is the side length of a cube to be scanned.
- The linear number of voxels, $r \in \mathbb{N}$, of the model used during 3D reconstruction. Our region is assumed to be a cube, so this is the side length of a virtual cube of voxels.
- A series of $i \ n \times m$ depth frames, $D^i \in \mathbb{R}^{+nm}$ provided by a camera. We assume each frame is generated from a camera by a noisy, physically realizable model.
- The camera intrinsic matrix, $K \in \mathbb{R}^{3 \times 3}$. The camera intrinsics provide information about the mapping from the values in a depth frame to the physical location of the surface that generated that reading [31].

During the scanning process a collection of voxels is stored as a cube of voxels. Each voxel stores the signed distance from each voxel to the nearest surface, which is then truncated if this distance is too large. The collection of voxels is known as the truncated signed distance function (TSDF) [8] volume. The number of voxels r^3 in the TSDF volume acts as a metric for the resolution of the reconstruction (see IV-B).

The depth frames are each a 2D matrix, with each value representing the depth to the nearest surface of a given ray. The camera intrinsic matrix is used to determine the angle of a given ray described by the depth map.

Each measurement in D^i is itself noisy with an unknown noise function. The core function of this algorithm is to integrate all measurements in D^i to determine the true generating model.

The algorithm outputs the following:

- A set V of vertices, consisting of elements $v^j \in \mathbb{R}^3$ for $j = [1, |V|]$. Each vertex is the physical location of a 3D point relative to the camera initialization location.
- A set N of normals, consisting of elements $n^j \in \mathbb{R}^3$ for $j = [1, |N|]$. n^j corresponds to the normal for vertex v^j .

We note that the magnitude of V is upper bounded by r^3 . That is, the number of vertices in the reconstruction cannot exceed the number of voxels in the model used for reconstruction.

B. Metrics

In the ideal case, each vertex represents the location of a surface, with location identical to that of a point on some surface relative to the initial camera location. To capture the error in these distance, we define the mean distance from each vertex to the nearest true surface as the *accuracy* of the model. As a second constraint, for each voxel in the reconstructive model, if a surface crosses through that voxel, then a vertex is created for that voxel. Increasing the number of vertices in the output will be defined as increasing the *resolution* of the model.

V. RECONSTRUCTION ALGORITHM

Those who are familiar with the KinectFusion algorithm will notice that the steps listed below follow a similar structure. The key modification with our algorithm is that it allows for the ability to increase the resolution of the reconstruction to a user specified degree in exchange for computation time.

A. Initialization

This algorithm allows for the number of voxels r^3 to be a user tunable parameter. However, future steps in our algorithm rely on being able to perform computation on the TSDF volume on a GPU. In the case where the user-provided r results in too many voxels for the entire volume to be stored in GPU memory, the TSDF volume will be broken into a set of TSDF subvolumes H . Each subvolume $h \in H$ acts as a TSDF volume and is used in reconstruction, but

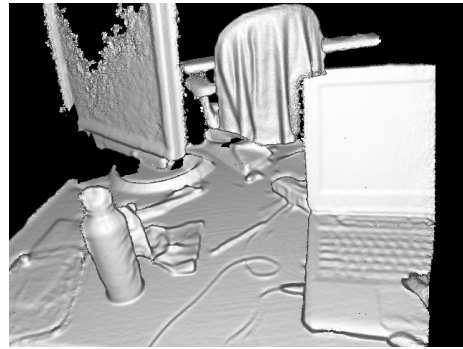


Fig. 3: Image generated from 4 1.5 meter TSDF subvolumes.

are separated so that computation can be performed on them independently.

We define r_{GPU} to be the maximum number of linear voxels that can fit into GPU memory. The linear number of TSDF subvolumes initialized is $\frac{r}{r_{\text{GPU}}}$.

The initial location of the camera is initialized as $(0, 0, 0)$. The back, center voxel of the TSDF volume is additionally initialized to this location. In order to achieve this, each subvolume is placed such that they form a cube with back center at $(0, 0, 0)$. Each subvolume stores the translation h_t of its back center voxel relative to $(0, 0, 0)$, its linear number of voxels h_r and its linear physical dimension h_l . For reasons mentioned Section V-F, each subvolume overlaps by two pixels, but this will be ignored for the majority of the analysis, as it only results in a constant factor decrease in the total volume size.

B. Depth Map Conversion

For each frame i , the depth map D^i is converted into a collection of vertices. A given vertex in coordinates of the current frame $v_l^i(x, y) = K^{-1}[x, y, 1]^T D^i(x, y)$ for pixel coordinates $x = [0, m - 1]$ and $y = [0, n - 1]$. This is done on the GPU on a per pixel basis. The normals are then computed for each vertex: $n_l^i(x, y) = (v_l^i(x + 1, y) - v_l^i(x, y)) \times (v_l^i(x, y + 1) - v_l^i(x, y))$.

Using the transformation matrix derived from the previous camera tracking iteration (see Section V-C), the global position of each point is then derived. The global transformation matrix $T^{i-1} = [R^{i-1} | t^{i-1}]$, with translation vector $t^{i-1} \in \mathbb{R}^3$ and rotation matrix $R^{i-1} \in SO(3)$. The global vertex location is then $v_i(x, y) = t^{i-1} + v_l^i(x, y)$ and global normal is $n_i(x, y) = R^{i-1} n_l^i(x, y)$. This puts our vertex in normals in the global coordinate frame defined, which is necessary for future steps.

C. Camera Tracking

The transformation matrix between the vertices derived from the previous raycasting step and the current depth map conversion step is determined. This is run by performing a GPU based iterative closest point (ICP) algorithm, the details of which can be found in [1]. The transformation is then applied to T^{i-1} to determine the current global transformation matrix T^i .

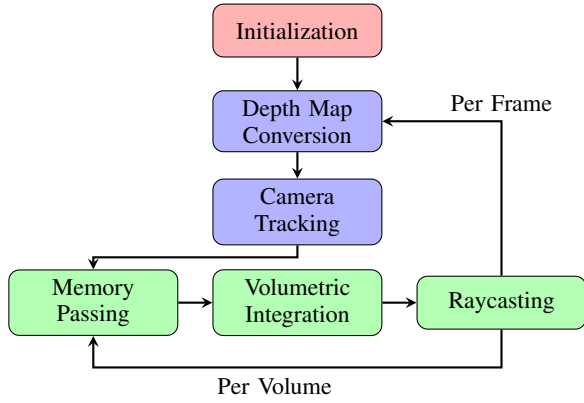


Fig. 4: Flowchart for model creation. At the beginning of each dataset, TSDF volumes are initialized. For each frame, the frames depth map is converted to global coordinates and the camera transformation from the previous frame to the current one. A volume is passed to GPU memory, where volumetric integration and raycasting are then performed to update our TSDF volumes and obtain the raycasted depth map. **Red:** Performed once per dataset. **Blue:** Performed once per frame. **Green:** Performed on each volume for each frame.

D. Memory Passing

To store the amount of data required to have multiple TSDF subvolumes, they generally need to be stored in CPU memory, as we constructed the subvolumes such that only one may fit in GPU memory. Generally a computer has many times more CPU memory than GPU memory. Because of this, and the benefits of virtual memory, we can store more volumes in CPU memory than in GPU memory (see section VI.B.). Prior to a volumetric integration step, one TSDF subvolume is uploaded to the GPU for point volumetric integration and raycasting. After raycasting, this volume is downloaded to CPU memory. This happens for each subvolume, upon which the final raycasting step is complete for that frame.

E. Volumetric Integration

During this step we update our TSDF subvolumes, which store our beliefs of which surfaces are relative to our global origin. Each subvolume h stores a set of values $h_d^i(t_l)$ where $t_l = (t_l^x, t_l^y, t_l^z) \in \mathbb{R}^3$ represents the voxel coordinate, and $h_d^i \in \mathbb{R}^3$ stores the believed distances to the nearest surface for each voxel in subvolume h on the i th frame.

Each GPU thread is assigned an (t_l^x, t_l^y) location, for $t_l^x = [0, r - 1]$ and $t_l^y = [0, r - 1]$. Each thread then iterates over each $t_l^z = [0, r - 1]$ for its given (t_l^x, t_l^y) . Each voxel’s distance to the nearest surface is determined using its t_l coordinate. However because each subvolume is translated relative to the origin by translation h_t , the coordinate to use to calculate distance is then $t_s = t_l + h_t$. From here the physical model distance is calculated as $d_m = \frac{1}{r} \|t_s\|$, which represents the distance from the camera origin to the voxel.

In order to determine the measured distance for that frame, each t_s voxel position is then back projected to pixel coordinates to get an (x, y) location. Using this the distance

to the nearest surface is calculated as $dist = D^i(x, y) - d_m$. $dist$ is then constrained to be within some truncation bounds proportional to the physical distance of a voxel in order to prevent unnecessary computation. From here we can calculate the updated TSDF value $h_d^i(t_l) = \frac{w^{i-1}h_d^{i-1}(t_l) + w^i dist}{w^{i-1} + w^i}$, for each voxel, which is the belief of the distance from that voxel to the nearest surface. w^i is a linearly increasing weighting function, up to some maximum.

F. Raycasting

During this step we derive the depth map constructed from our TSDF volume. As mentioned above, the raycasting step is run once separately per subvolume, each after the matching volumetric integration step.

Prior to the memory passing step a pixel distance map $v_r \in \mathbb{R}^+$ and normal map $n_r \in \mathbb{R}^{+3}$, each of size $m \times n$ are initialized. Based on the camera intrinsics, a ray can be cast from each pixel location (x, y) in the camera space through the TSDF volume. As each ray iterates through the TSDF volume space, checks for the value of the TSDF voxel it is currently in. If the ray passes through a change of sign between voxels, it is noted to have crossed through a surface. By trilinearly interpolating over the voxels on either side of the zero-crossing, the location of the surface is determined. Because the side of each voxel is known, the raycasted voxel location $v_r(x, y)$ is determined. Similarly the derivative of the TSDF as the zero-crossing is used to determine the normal value $n_r(x, y)$ for this pixel.

However because we are only working on a given subvolume, a few modifications need to be made. While raycasting, calculation is only done while the ray is within the TSDF subvolume, or until it finds a zero-crossing. As a ray is cast from a camera location, its voxel position in global space can be described as a position $t_r \in \mathbb{R}^3$. The voxel position in volume coordinates is then $t'_r = t_r - h_t$. We then read values of the voxels at t'_r when searching for zero crossing. When determining the global physical locations g of each voxel, the translations must be added back to our new indices, to accurately reflect the physical distance the ray travels to our translated volume. This gives us $g = h_l * (t'_r + h_t)$. When a zero crossing is found, the value is trilinearly interpolated over neighboring voxels to determine $v_r(x, y)$, and the derivative of the TSDF at the zero crossing is calculated to determine $v_n(x, y)$.

It is worth noting that all raycasting steps modify the same map. This means each pixel coordinate is searched over by each subvolume, even though all edit the same map. In order to guarantee that we use the correct value in our voxel map, we take the value with the shortest raycast distance from the local camera location. This guarantees that we always take the value of the surface visible by the current camera location. To trilinearly interpolate successfully each subvolume must overlap by 2 voxels.

G. Comparison to KinectFusion

We show that when creating a cube of multiple volumes the results are identical to that of running the KinectFusion

algorithm on one volume with the same total number of voxels. Because the volumetric integration and raycasting steps are the only ones modified, if we can show they give identical outputs to KinectFusion, then the entire algorithm also does so. For sake of simplicity we will ignore the overlapping voxels in our volumes when discussing the number of voxels, which is accounted for by requiring that each volume be larger by the size of 2 voxels.

During the volumetric integration step, each voxel is independent of each other voxel. That is, the calculation performed only depends on the TSDF value of the given voxel, and the depth of the ray back projected from that voxel. All modifications done by our algorithm guarantee that the voxel is associated with the correct physical location, but do not affect the TSDF value or the depth value. Due to the fact that all computation depends on each voxel independently, that voxels exist in separate volumes does not affect the correctness of the computation.

In the raycasting step, unlike the volumetric integration step, the voxels are not independent. Due to trilinear interpolation, each voxel depends on each neighboring voxel. However given that the volumetric integration step is identical to KinectFusion, upon overlapping the volumes, the overlapping voxels will have identical values. Therefore during the trilinear interpolation step, every voxel for which trilinear interpolation is possible will have a set of neighbors identical to that of KinectFusion. By then only using the shortest distance zero-crossing found by each ray, the depth and normal maps are identical to those in KinectFusion.

H. Benefits

This algorithm is designed explicitly to create high-resolution volumes of a fixed area. By using the TSDF volume techniques of KinectFusion we create a more accurate 3D model than any individual frame. Then by allowing for a number of subvolumes, and thereby voxels, only bounded by disk space, we allow for resolution functionally bounded only by the noise in the camera which generates the depth frames. This is compared to the resolution bounded by GPU size in KinectFusion.

VI. DYNAMIC VOLUME ALLOCATION

Our goal is again to create a 3D reconstruction of a noisy measurement model while optimizing over accuracy and resolution. However in this case we present the additional requirement that resolution of the model in a given region be variable based on user input.

A. Input and Output

The output relationship of dynamic allocation is identical to that of the high-resolution reconstruction.

During runtime the algorithm will keep a list H of active subvolumes it is processing on. Each subvolume $h \in H$ is initialized by 3 parameters: h_l , the linear physical dimension, h_r , the linear number of voxels, and h_t , the translation relative to the camera origin. A volume can be added to the set at any point during execution, and will be processed in



Fig. 5: Volumes can be placed anywhere relative to the initial camera location. Here we scan with three spaced out volumes, and choose not to allocate a volume in the bottom left corner for demonstration purposes.

subsequent frames. To remove a volume from processing, it is removed from the set of volumes. The point cloud for the removed volume can then be downloaded to main memory. Thus the additional input parameters are:

- $f(\cdot)$, which can take in any data available during a given frame. It returns a list of volume parameters (h_p^1, \dots, h_p^n) for the volumes to be added, where $h_p = (h_l, h_r, h_t)$ for some subvolume.
- $g(h, \cdot)$, which is run for all $h \in H$. The function removes the volume from H if the conditions it specifies are met. It can additionally take in any other parameters available in the system.

By defining f and g , this algorithm can be extended to a multitude of use cases. For example, the work of Kaparthi *et al.* [5] could be applied to create higher resolution models for areas with object-like properties.

B. Insertion and Removal

After the final raycasting step an additional insertion and removal step is added. During this step the removal algorithm $f(\cdot)$ is first run. Each subvolume to be added is specified with h_l , the linear physical dimension, h_r , the linear number of voxels, and h_t , the translation relative to the camera original. Each subvolume specified by $f(\cdot)$ is then marked for addition.

$g(h, \cdot)$ is then run for each $h \in H$. Note that this algorithm can use any parameter of the algorithm, including the set of subvolumes marked for addition. If a subvolume specified has identical parameters to one marked for addition, that volume instead will not be marked for addition. This provides a mechanism for $f(\cdot)$ and $g(h, \cdot)$ to interact. Each subvolume specified is then marked for addition.

Because each TSDF volume can be described as a point cloud, the volumes marked for deletion have their point cloud representations downloaded to CPU memory. The volumes marked for addition are then added to H , and used during the volumetric integration and raycasting steps of future iterations.

C. Dynamic Mapping for SLAM

To perform large-scale mapping we propose a tool for dynamically placing subvolumes in areas expected to have a high density of surface vertices. There are three tunable

Algorithm 1 The update steps performed for each volume.

```

1: procedure VOLUME UPDATE( $h, D, v_r, n_r$ )
2:   uploadToGPU( $h$ )
3:   for  $(x, y)$  in  $([0, r - 1], [0, r - 1])$  do
4:     for  $z$  in  $[0, r - 1]$  do
5:        $t_s \leftarrow t_l + h_t$ 
6:        $(x, y) \leftarrow \text{backProject}(t_s)$ 
7:        $dist \leftarrow D^i(x, y) - \frac{1}{r} \|t_s\|$ 
8:        $h_d(t_l)^i \leftarrow \text{updateWeight}(h, x, y, dist)$ 
9:     end for
10:  end for
11:  for  $(x, y)$  in  $([0, r - 1], [0, r - 1])$  do
12:     $t_r \leftarrow \text{castRay}(x, y, (0, 0, 0)) - h_t$ 
13:     $t'_r \leftarrow t_r - h_t$ 
14:    while inVolume( $t_r - h_t$ ) do
15:       $t_r \leftarrow \text{castRay}(x, y, t_r) - h_t$ 
16:       $t'_r \leftarrow t_r - h_t$ 
17:      if zeroCrossing( $t'_r$ ) then
18:         $g \leftarrow h_l * (t'_r + h_t)$ 
19:         $v_r(x, y) \leftarrow \text{calculateVertex}(g)$ 
20:         $v_n(x, y) \leftarrow \text{calculateNormal}(g)$ 
21:      end if
22:    end while
23:  end for
24:  uploadToCPU( $h$ )
25: end procedure

```

parameters in this system: The linear number of voxels in each TSDF subvolume d_v , the linear physical dimension in each subvolume d_l , and the maximum number of subvolumes to exist at once time n . Our system dynamically places n subvolumes h each with $h_l = d_l$ and $h_v = d_v$ in locations based on the following process.

We define the origin of the global coordinate frame as the initial location of the camera. Assuming voxels of fixed size, we can view this coordinate system as having length units in voxels rather than a physical length. We allow subvolumes to be placed on this coordinate system such that their translations from the origin are constrained to $h_t = k * (d_v - 2)$, where $k \in \mathbb{Z}^3$. This allows the subvolumes to be placed on a 3D grid, where each cell is the size of a subvolume. The (-2) term is so that adjacent cubes do not create a gap in the raycasting result and will be excluded for simplicity of notation. We do not allow multiple subvolumes to have the same translation, so a subvolume’s placement in this grid defines a unique property of the subvolume.

During the raycasting operation, for each pixel $p = D^i(x, y)$ in the depth frame, we calculate the the endpoint $e = (e^x, e^y, e^z) \in \mathbb{R}^3$ of the ray generated from p based on the depth r_d and direction $r_v = (r_v^x, r_v^y, r_v^z) \in \mathbb{R}^3$ from p . Using this we calculate the location in global coordinates of where that depth value maps.

$$e^x = \frac{r_v^x}{\sqrt{\left(\frac{r_v^z}{r_v^x}\right)^2 + \left(\frac{r_v^y}{r_v^x}\right)^2 + 1}}$$

$$e^y = \frac{r_v^y}{r_v^x} * x, e^z = \frac{r_v^z}{r_v^x} * x$$

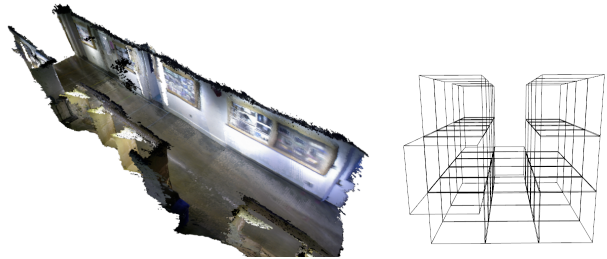


Fig. 6: **Left:** Scan of hallway. This scan was taken while simply walking forward, yet still captures both walls and the floor at high resolution. 2m subvolume were dynamically allocated such that at most 16 were live at one time. This image consists of 24 subvolumes. **Right:** Volume placement on a short hallway scene. We see no subvolumes allocated in the region between the walls.

We then convert each endpoint to a coordinate l which is constrained to $h_t = k * (d_v)$ as the subvolume locations are $l = \left(\frac{e^x, e^y, e^z}{d_l}\right) - \left(\frac{e^x, e^y, e^z}{d_l} \bmod d_v\right)$

Any ray with endpoint l maps uniquely to a subvolume. We define $c(l)$ as the number of rays that end at the subvolume mapped to l . The set L is defined as all subvolume locations with non-zero $c(l)$. Our insertion function takes in the current subvolume set H and all $c(l)$ for $l \in L$, so the function signature is $f(H, L, c(L))$. We then only keep the subvolumes with the N largest $c(l)$ values. Our removal function $g(h, \cdot)$ removes a subvolume which has been marked as having falling out of the top n subvolumes. In order to prevent volumes from switching in and out too often, we also set a threshold that a subvolume to be added needs to have a count larger than the lowest count subvolume by some constant factor.

VII. EXPERIMENTS

The key benefit of our algorithm is the ability to increase the resolution of our model without sacrificing accuracy, but at the cost of computation time. Therefore to quantitatively evaluate our algorithm we use two metrics:

- Runtime performance of the algorithm as a function of the number of TSDF volumes being used.
- Comparison against the PCL implementation of KinectFusion (KinFu) [9] using benchmarks developed by [7].

We further discuss qualitative results of our algorithm.

VIII. HARDWARE

Our computer uses an nVidia GeForce GTX 880M graphics card with 8GB GPU memory, along with a 2.7GHz Intel Core i7 4800MQ processor. It has 32GB main memory, along with a 1TB SSD. We allocated an additional 64GB of swap space in order to guarantee the function of our algorithm. We used an ASUS Xtion Pro camera for all experiments.

IX. RUNTIME PERFORMANCE

The fundamental tradeoff of our algorithm is speed versus resolution. As the number of volumes we use increases we expect the time transferring data from GPU memory to CPU memory to account for the majority of the processing time. Because this happens for every volume on each frame, we

TABLE I: Model to Ground-Truth Error

| | traj0 | traj1 | traj2 |
|----------------------------|---------|---------|---------|
| KinFu Volume | | | |
| vertices(m) | 1497300 | 1465488 | 506229 |
| mean(m) | 0.0309 | 0.0534 | 0.0213 |
| median(m) | 0.0215 | 0.0375 | 0.0134 |
| std(m) | 0.0282 | 0.0542 | 0.0254 |
| Eight Dense Volumes | | | |
| vertices | 7318191 | 7354923 | 2192196 |
| mean(m) | 0.0335 | 0.0537 | 0.0222 |
| median(m) | 0.0253 | 0.0368 | 0.0152 |
| std(m) | 0.0315 | 0.0545 | 0.0250 |

expect the time to be linear with the number of volumes, until the computer switches to swap memory.

We ran the following experiment to validate our runtime expectations. On a pre-recorded 100 frame real world dataset we dynamically allocated a fixed number of volumes with 512 linear voxels on the first frame. For 2 to 7 volumes we used 1.5m volumes. In order to guarantee there existed unique data for each volume, we decreased the size of each volumes as the number of volumes increased.

Our results show the seconds per frame is linear with the number of volumes, with each volume adding approximately .17s per frame. By running the algorithm with 48 volumes we demonstrate the ability to generate a 48x increase in resolution compared to a single volume. We also found that both PCL KinFu and our implementation ran at approximately 11 frames per second for one volume. It is worth noting that this is less than the expected 30 frames per second because the images were read out of memory instead of a live camera feed. At 64 volumes the computer begins using swap memory, and the time increases to approximately 150 seconds per frame.

X. COMPARISON WITH BASELINE

We compare our algorithm to PCL KinFu on the synthetic dataset developed by Handa *et al.* [7]. This dataset provides a series of RGB and Depth frames that are structured simulate the camera movement through a virtual living room. Also provided is an .obj model for each dataset as ground truth. In order to accurately simulate a depth camera, Handa *et al.* added noise as described in [32] to each frame.

For our experiments we limited the range of camera scenes to those contained by a 6m KinectFusion volume. For the experiments we ran each mapping algorithm on a scene in order to generate a 3D map. We then use the open source Cloud Compare¹ to align the reconstruction to the ground truth model. This provides the translation of each point in the reconstruction relative to the nearest mesh triangle in the ground truth model. Using the statistics provided by [7], we then determine the mean, median, and standard deviation for each reconstruction’s translation, the results of which can be seen in Table 1. For traj0 and traj1 we ran PCL KinFu with a 6m volume size, and our algorithm with a set of 8 volumes forming a cube of 6m (3m per volume). For traj2 we ran PCL KinFu with a 3m volume size, and our algorithm with a set of 8 volumes forming a cube of 3m (so 1.5m per volume). All trajectories used 512 linear voxels per volume.

¹<http://www.danielgm.net/cc/>



Fig. 7: **Top:** Fireplace scene at the Kendall Hotel in Cambridge, MA. **Bottom:** Zoom of two busts from the same model. Model was generated using dynamically placed .75m volumes. The color misalignment is due to a misalignment in the colors with the 3D model, and is not an issue with the 3D model itself.

Table 1 shows that our algorithm generates on average 4.75 times as many vertices, indicating a 4.75 time increase in resolution by our definition. Reconstruction accuracy is in line with KinFu, with the average mean error increased by 4.2%. Due to the relatively small number of points used to generate the synthetic meshes, we do not expect to see an improvement in model reconstruction statistics relative to KinectFusion, even for large volumes, due to the fact the synthetic dataset is almost entirely flat surfaces, reconstruction resolution has a minor impact on error. Given the small difference in quality and high number of vertices increased, we believe this highlights the algorithm’s ability to generate high-resolution datasets without reducing accuracy. As a matter of future work it would be useful to generate a dense synthetic dataset and determine if our model reduces mesh reconstruction error.

XI. QUALITATIVE RESULTS

We tested our dynamic volume allocation with 3m volumes while walking down a hallway, as seen in Figure 6. To obtain this dataset the camera was not rotated as it

was translated through the hallway, highlighting the ability to obtain large scale datasets easily. We found that large datasets like this often had drift due to accumulated error in ICP, which can be resolved by future work improving visual odometry.

The fireplace seen in Figure 7 highlights power of our algorithm. The figure was generated by a 40 second scan of the fireplace and mantelpiece. By acting on a "medium" scale scan such as this, we do not see the sensor drift present in hallway scans. Additionally this highlights how a large area can be scanned in high resolution, while we still see the detail in the individual busts.

XII. CONCLUSION

In this paper, we presented a novel method for high resolution, spatially extended RGB-D mapping. Our algorithm uses multiple mapping volumes balanced between the CPU and GPU to provide higher resolution than current state-of-the-art mapping systems. We also presented a method for dynamically adding and removing mapping volumes to allow for spatially extended mapping. We evaluated our method on multiple indoor and simulated datasets and showed results for a 48x increase in resolution over current state-of-the-art mapping. Furthermore, the dynamic placement of mapping volumes allows for the choice of mapping areas of interest, which can be object-centric or for full scene reconstruction.

REFERENCES

- [1] R. A. Newcombe, A. J. Davison, S. Izadi, P. Kohli, O. Hilliges, J. Shotton, D. Molyneaux, S. Hodges, D. Kim, and A. Fitzgibbon, "KinectFusion: Real-time dense surface mapping and tracking," in *IEEE and ACM Intl. Sym. on Mixed and Augmented Reality (ISMAR)*, (Basel, Switzerland), pp. 127–136, Oct. 2011.
- [2] T. Whelan, M. Kaess, J. Leonard, and J. McDonald, "Deformation-based loop closure for large scale dense RGB-D SLAM," in *IEEE/RSJ Intl. Conf. on Intelligent Robots and Systems (IROS)*, (Tokyo, Japan), Nov. 2013.
- [3] H. Roth and M. Vona, "Moving volume KinectFusion," in *British Machine Vision Conf. (BMVC)*, Sept. 2012.
- [4] R. Finman, T. Whelan, M. Kaess, and J. Leonard, "Toward lifelong object segmentation from change detection in dense RGB-D maps," in *European Conference on Mobile Robotics*, (Barcelona, Spain), Sept. 2013.
- [5] A. Karpathy, S. Miller, and L. Fei-Fei, "Object discovery in 3D scenes via shape analysis," in *International Conference on Robotics and Automation (ICRA)*, 2013.
- [6] R. Wagner, U. Frese, and B. Bäuml, "3D Modeling, Distance and Gradient Computation for Motion Planning: A Direct GPGPU Approach," in *International Conference on Robotics and Automation (ICRA)*, 2013.
- [7] A. Handa, T. Whelan, J. McDonald, and A. Davison, "A benchmark for RGB-D visual odometry, 3D reconstruction and SLAM," in *IEEE Intl. Conf. on Robotics and Automation, ICRA*, (Hong Kong, China), May 2014. (to appear).
- [8] B. Curless and M. Levoy, "A volumetric method for building complex models from range images," in *SIGGRAPH*, pp. 303–312, Aug. 1996.
- [9] R. Rusu and S. Cousins, "3D is here: Point Cloud Library (PCL)," in *IEEE Intl. Conf. on Robotics and Automation (ICRA)*, (Shanghai, China), May 2011.
- [10] A. Comport, E. Malis, and P. Rives, "Accurate Quadri-focal Tracking for Robust 3D Visual Odometry," in *IEEE International Conference on Robotics and Automation, ICRA'07*, (Rome, Italy), April 2007.
- [11] J. Engel, T. Schöps, and D. Cremers, "LSD-SLAM: Large-scale direct monocular SLAM," in *Computer Vision—ECCV 2014*, pp. 834–849, Springer, 2014.
- [12] R. Newcombe, S. Lovegrove, and A. Davison, "DTAM: Dense tracking and mapping in real-time," in *Intl. Conf. on Computer Vision (ICCV)*, (Barcelona, Spain), pp. 2320–2327, Nov. 2011.
- [13] G. Klein and D. Murray, "Parallel tracking and mapping for small AR workspaces," in *IEEE and ACM Intl. Sym. on Mixed and Augmented Reality (ISMAR)*, (Nara, Japan), pp. 225–234, Nov. 2007.
- [14] M. Zeng, F. Zhao, J. Zheng, and X. Liu, "A Memory-Efficient Kinect-Fusion Using Octree," in *Computational Visual Media*, vol. 7633 of *Lecture Notes in Computer Science*, pp. 234–241, Springer, 2012.
- [15] Q. Zhou and V. Koltun, "Dense scene reconstruction with points of interest," in *SIGGRAPH 2013*, (Anaheim, CA, USA), ACM, 2013.
- [16] Q. Zhou, S. Miller, and V. Koltun, "Elastic Fragments for Dense Scene Reconstruction," in *Intl. Conf. on Computer Vision (ICCV)*, December 2013.
- [17] D. R. Canelhas, T. Stoyanov, and A. J. Lilienthal, "SDF Tracker: A parallel algorithm for on-line pose estimation and scene reconstruction from depth images," in *IEEE/RSJ Intl. Conf. on Intelligent Robots and Systems, IROS*, (Tokyo, Japan), November 2013.
- [18] K. Pirker, M. Rütger, G. Schweighofer, and H. Bischof, "GPSlam: Marrying sparse geometric and dense probabilistic visual mapping," in *British Machine Vision Conf. (BMVC)*, Aug. 2011.
- [19] J. Stückler and S. Behnke, "Multi-resolution surfel maps for efficient dense 3D modeling and tracking," in *Journal of Visual Communication and Image Representation*, 2013.
- [20] P. Henry, M. Krainin, E. Herbst, X. Ren, and D. Fox, "RGB-D mapping: Using Kinect-style depth cameras for dense 3D modeling of indoor environments," *Intl. J. of Robotics Research*, vol. 31, no. 5, pp. 647–663, 2012.
- [21] F. Endres, J. Hess, N. Engelhard, J. Sturm, D. Cremers, and W. Burgard, "An evaluation of the RGB-D SLAM system," in *IEEE Intl. Conf. on Robotics and Automation (ICRA)*, 2012.
- [22] T. Tykkälä, A. I. Comport, and J.-K. Kamarainen, "Photorealistic 3D Mapping of Indoors by RGB-D Scanning Process," in *International Conference on Intelligent Robots and Systems*, (Tokyo, Japan), 3-7 November 2013.
- [23] M. Meilland and A. Comport, "On unifying key-frame and voxel-based dense visual SLAM at large scales," in *International Conference on Intelligent Robots and Systems*, (Tokyo, Japan), IEEE/RSJ, 3-8 November 2013.
- [24] M. Meilland, T. Drummond, and A. Comport, "A Unified Rolling Shutter and Motion Model for Dense 3D Visual Tracking," in *International Conference on Computer Vision*, (Sydney, Australia), December 3-6 2013.
- [25] M. Meilland and A. I. Comport, "Super-resolution 3d tracking and mapping," in *Robotics and Automation (ICRA), 2013 IEEE International Conference on*, pp. 5717–5723, IEEE, 2013.
- [26] F. Steinbrücker, C. Kerl, J. Sturm, and D. Cremers, "Large-scale multi-resolution surface reconstruction from RGB-D sequences," in *IEEE International Conference on Computer Vision (ICCV)*, (Sydney, Australia), 2013.
- [27] K. M. Wurm, A. Hornung, M. Bennewitz, C. Stachniss, and W. Burgard, "OctoMap: A probabilistic, flexible, and compact 3D map representation for robotic systems," in *Proc. of the ICRA 2010 Workshop on Best Practice in 3D Perception and Modeling for Mobile Manipulation*, (Anchorage, AK, USA), May 2010.
- [28] J. Chen, D. Bautembach, and S. Izadi, "Scalable real-time volumetric surface reconstruction," *ACM Trans. Graph.*, vol. 32, pp. 113:1–113:16, July 2013.
- [29] M. Nießner, M. Zollhöfer, S. Izadi, and M. Stamminger, "Real-time 3d reconstruction at scale using voxel hashing," *ACM Trans. Graph.*, vol. 32, pp. 169:1–169:11, Nov. 2013.
- [30] P. Henry, D. Fox, A. Bhowmik, and R. Mongia, "Patch Volumes: Segmentation-based Consistent Mapping with RGB-D Cameras," in *Third Joint 3DIM/3DPVT Conference (3DV)*, 2013.
- [31] R. Hartley and A. Zisserman, *Multiple View Geometry in Computer Vision*. Cambridge University Press, 2003. Second Edition.
- [32] J. T. Barron and J. Malik, "Intrinsic scene properties from a single RGB-D image," in *Computer Vision and Pattern Recognition (CVPR), 2013 IEEE Conference on*, pp. 17–24, IEEE, 2013.